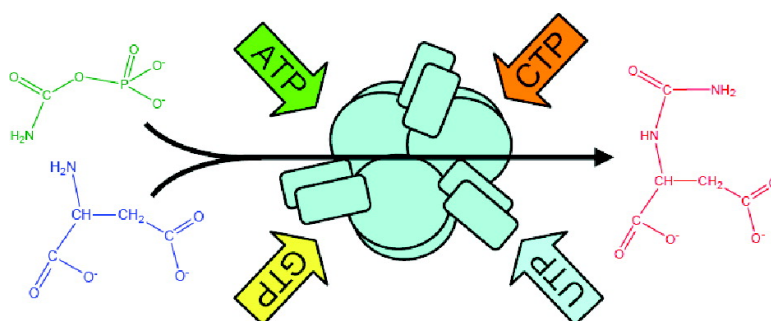Article

Dissecting Enzyme Regulation by Multiple Allosteric Effectors: Nucleotide Regulation of Aspartate Transcarbamoylase

Joshua D. Rabinowitz, Jennifer J. Hsiao, Kimberly R. Gryncel, Evan R. Kantrowitz, Xiao-Jiang Feng, Genyuan Li, and Herschel Rabitz

More About This Article

Additional resources and features associated with this article are available within the HTML version:

- Supporting Information
- Access to high resolution figures
- Links to articles and content related to this article
- Copyright permission to reproduce figures and/or text from this article

View the Full Text HTML

Dissecting Enzyme Regulation by Multiple Allosteric Effectors: Nucleotide Regulation of Aspartate Transcarbamoylase[†]

Joshua D. Rabinowitz,*[,‡,§] Jennifer J. Hsiao,[‡,§] Kimberly R. Gryncel,[∥] Evan R. Kantrowitz,[∥] Xiao-Jiang Feng,[‡] Genyuan Li,[‡] and Herschel Rabitz[‡]

Department of Chemistry, Princeton University, Princeton, New Jersey 08544, Lewis-Sigler Institute for Integrative Genomics, Princeton, New Jersey 08544, and Department of Chemistry, Boston College, Merkert Chemistry Center, Chestnut Hill, Massachusetts 02467

ABSTRACT: The enzyme aspartate transcarbamoylase (ATCase, EC 2.1.3.2 of *Escherichia coli*), which catalyzes the committed step of pyrimidine biosynthesis, is allosterically regulated by all four ribonucleoside triphosphates (NTPs) in a nonlinear manner. Here, we dissect this regulation using the recently developed approach of random sampling−high-dimensional model representation (RS−HDMR). ATCase activity was measured *in vitro* at 300 random NTP concentration combinations, each involving (consistent with *in vivo* conditions) all four NTPs being present. These data were then used to derive a RS−HDMR model of ATCase activity over the full four-dimensional NTP space. The model accounted for 90% of the variance in the experimental data. Its main elements were positive ATCase regulation by ATP and negative by CTP, with the negative effects of CTP dominating the positive ones of ATP when both regulators were abundant (i.e., a negative cooperative effect of ATP × CTP). Strong sensitivity to both ATP and CTP concentrations occurred in their physiological concentration ranges. UTP had only a slight effect, and GTP had almost none. These findings support a predominant role of CTP and ATP in ATCase regulation. The general approach provides a new paradigm for dissecting multifactorial regulation of biological molecules and processes.

Many biochemical processes are sensitive to multiple signals, which may interact in a nonlinear manner. While such sensitivity often arises from complex reaction networks, even single enzymes can respond to multiple regulators. One such enzyme is aspartate transcarbamoylase (ATCase) (*1*), a complex in which activity and regulation are on distinct polypeptide chains (*2*). ATCase is composed of 12 polypeptides (6 c chains and 6 r chains), organized as two catalytic trimers bound to three regulatory dimers (*3, 4*). It catalyzes the first committed step in the metabolic pathway for *de novo* pyrimidine biosynthesis: the condensation of aspartate with carbamoyl phosphate to yield carbamoyl aspartate. Binding of substrate to the enzyme is ordered, with carbamoyl phosphate binding before aspartate (*5, 6*) and inducing local conformational changes leading to the formation of a viable aspartate-binding site (*7*).

Both genetic and biochemical evidence support CTP, a primary end product of the pathway, being the key negative regulator of ATCase (a classical example of feedback inhibition) (*8*). Biochemical evidence also demonstrates that ATP substantially enhances enzyme activity (*9*), with this regulation serving to balance pyrimidine and purine concentrations. Crystal structures of the ATCase complex have been solved with ATP or CTP bound and confirm that ATP and CTP bind to and induce conformational changes in the regulatory subunits (*10–18*). Quantitative modeling of the enzyme activity as a function of ATP and CTP binding has been performed and generally agrees with the classical model of Monod et al. (*19*), in which the enzyme complex exists in either a T (tense and less active) or R (relaxed and more active) state, with the transition between the two states sensitive to ATP, CTP, and substrate concentrations (*12, 20–22*).

While the regulatory roles of CTP and ATP have been extensively studied, recent work has suggested a role also for UTP as a feedback inhibitor, both weakly on its own and synergistically with CTP (*23*). Studies with GTP have shown it to have an inhibitory effect on its own but sometimes a stimulatory effect in combination with other nucleotides (*24*). Although these interactions have been incorporated in some quantitative models of the pyrimidine pathway (e.g., ref *25*), their significance remains unclear. Nevertheless, their discovery points to the importance of moving from studying the responses of ATCase to single nucleotides in isolation to consideration of the more physiological situation in which all four NTPs are present simultaneously. A challenge in this regard has been the absence of methods for mapping nonlinear functions of many

* To whom correspondence should be addressed: 241 Carl Icahn Laboratory, Princeton University, Princeton, NJ 08544. Telephone: 609-258-8985. Fax: 609-258-3565. E-mail: joshr@princeton.edu.
[‡] Princeton University.
[§] Lewis-Sigler Institute for Integrative Genomics.
[∥] Boston College.

variables that can be readily and reliably applied to biochemical systems.

A recently developed tool that holds promise for mapping input−output behavior is high-dimensional model representation (HDMR) (*26–28*). The impact of the multiple inputs on the output typically includes both independent and cooperative elements. These are captured in HDMR by approximating the output function $f(x)$, where $x = (x_1, x_2, ..., x_n)$ and x_i = value of the *i*th input, as a sum of component functions. The component functions include a zero-order function f_0 that is the mean output value, a maximum of n first-order functions $f_i(x_i)$ that describe the independent effects of the n input variables, a maximum of $n(n − 1)/2$ second-order functions that describe the cooperative effects of two input variables, etc. Component functions are added in a hierarchical manner (i.e., starting with the zero-order function, then adding first-order functions, etc.) only when they significantly improve the description of the overall input−output relationship. For most physical systems, approximation to the second or at most third order is adequate to capture the system behavior.

Importantly, the HDMR expansion has a straightforward statistical and physical interpretation: while $f(x)$ is impossible to visualize using standard graphical techniques for functions of $n \geq 3$ variables, the first- and second-order HDMR terms are readily plotted, and thus, the contributions of the different inputs, even for $n \geq 3$, can be dissected in a digestible form. In addition, the importance of the contributions associated with the different HDMR terms is encapsulated simply by the fraction of the variance of $f(x)$ that they capture.

While many different methods of sampling the high-dimensional input space can be applied to gather the data used to drive the HDMR analysis, one of the simplest and most reliable is random sampling (RS). Here, we apply RS−HDMR to investigate the effects of the four different ribonucleoside triphosphates on ATCase activity in the presence of fixed substrate concentrations [saturating carbamoyl phosphate; subsaturating aspartate at its typical intracellular concentration of 2.5 mM (*29*)]. We identify a second-order HDMR expression with good predictive reliability over the full NTP concentration space, with the predominant regulatory effects coming from ATP, CTP, and their interaction. These results both provide insight into the regulation of ATCase under the physiologically relevant condition of the four most abundant *Escherichia coli* NTPs being present and demonstrate the utility of HDMR in the analysis of biochemical systems.

MATERIALS AND METHODS

Enzyme and Reagents. Wild-type *E. coli* ATCase was expressed and purified as previously described (*30*). The enzyme concentration was determined by the Bradford assay, and the purity of the enzyme was confirmed using nondenaturing polyacrylamide gel electrophoresis (PAGE) and sodium dodecyl sulfate (SDS)−PAGE. NTPs, aspartate, and carbamoyl phosphate were purchased from Sigma.

ATCase Activity Assay. All reactions were carried out at pH 7.0 and 25 °C in 1 mL volume of 0.1 M imidazole buffer as previously described (*31*). Nucleotides were added from pH 7.0 stock solutions that were stored at −80 °C until immediately prior to use. Each reaction mixture contained

0.125 μg/mL aspartate transcarbamoylase, 2.5 mM aspartate, and selected concentrations of each of ATP, CTP, GTP, and UTP. The reaction was initiated by the addition of 4.8 mM carbamoyl phosphate. Given the ordered mechanism of the ATCase reaction (with carbamoyl phosphate binding before aspartate) and the use of saturating carbamoyl phosphate concentrations here, the present assay effectively probes the steps subsequent to initial carbamoyl phosphate binding only.

After 16 min of incubation, the reaction was terminated by the addition of color reagent (2 parts 5 g L^{-1} antipyrine in 50% sulfuric acid to 1 part 8 g L^{-1} 2,3-butanedionemonoxime in 5% acetic acid). After 16 h of incubation in the dark, the reaction mixture was incubated at 45 °C for 24 min under a fluorescent lamp to allow for color development. The mixture was then cooled to 4 °C on ice, and the absorbance (Abs) was measured at 466 nm. On each assay day, duplicate samples with no NTP added (standard) and lacking both NTPs and aspartate (blank) were also run. The normalized activity of ATCase in the presence of each NTP mixture was calculated as

$$\text{normalized activity} = (\text{Abs}_{\text{test sample}} - \text{Abs}_{\text{blank}})/$$
$$(\text{Abs}_{\text{standard}} - \text{Abs}_{\text{blank}}) \quad (1)$$

where $\text{Abs}_{\text{blank}}$ and $\text{Abs}_{\text{standard}}$ are the average of the measured values on the particular assay day.

Because the RS−HDMR modeling process effectively averages across all experimental results, only one measurement was taken for each individual data point used for RS−HDMR modeling (i.e., instead of aiming to reduce measurement error by taking repeated measurements of individual data points, we opted to reduce error, while also increasing coverage of the NTP concentration space, by drawing a large sample of data points). To determine the typical experimental error, normalized ATCase activity at four randomly selected NTP concentration combinations was measured repeatedly (eight replicates for each concentration combination). The mean standard deviation of these measurements was 0.09 normalized activity units.

Random Sampling of NTP Input Space. The four-dimensional NTP input space was sampled by random selection of 300 NTP concentration combinations using a computational random number generator. For ease of experimental implementation, the concentration of each NTP was selected from the following set: 0.01, 0.032, 0.1, 0.32, 1, 3.2, and 10 mM. NTP concentrations were log-transformed prior to RS−HDMR modeling. The samples are uniformly distributed with the log-transformed NTP concentrations.

RS−HDMR Modeling. The full RS−HDMR model considered was

$$f(x) \approx f_0 + f_1([\text{ATP}]) + f_2([\text{CTP}]) + f_3([\text{UTP}]) + f_4([\text{GTP}]) +$$
$$f_{12}([\text{ATP}], [\text{CTP}]) + f_{13}([\text{ATP}], [\text{UTP}]) +$$
$$f_{14}([\text{ATP}], [\text{GTP}]) + f_{23}([\text{CTP}], [\text{UTP}]) +$$
$$f_{24}([\text{CTP}], [\text{GTP}]) + f_{34}([\text{UTP}], [\text{GTP}]) +$$
$$f_{123}([\text{ATP}], [\text{CTP}], [\text{UTP}]) + f_{124}([\text{ATP}], [\text{CTP}], [\text{GTP}]) +$$
$$f_{134}([\text{ATP}], [\text{UTP}], [\text{GTP}]) + f_{234}([\text{CTP}], [\text{UTP}], [\text{GTP}]) +$$
$$f_{1234}([\text{ATP}], [\text{CTP}], [\text{UTP}], [\text{GTP}]) \quad (2)$$

where [NTP] refers to the log-transformed, normalized concentration of the NTP. NTP concentrations were normalized such that $x \in K^4$, where K^4 is the four-dimensional unit

hypercube. The normalization placed all inputs in RS−HDMR to be over a common range. The implementation of normalization was such that

$$[NTP_{used\ in\ modeling}] = (1/3)\log_{10}([NTP_{absolute}]/[0.01\ mM]) \tag{3}$$

Unless otherwise indicated, results are reported using standard millimolar NTP concentrations (obtained by solving eq 3 for $[NTP_{absolute}]$).

The HDMR component functions used were represented by orthonormal polynomial expansions. The advantage of using orthonormal polynomials as basis functions is that adding a new orthonormal polynomial into an expansion will always improve the accuracy. These polynomials were constructed by first identifying orthonormal polynomial basis functions (φ_{ir}) of variable x_i and degree $r \leq 2$, e.g.,

$$\varphi_{11}([ATP]) = \alpha_{11} + \beta_{11}[ATP] \tag{4a}$$

$$\varphi_{12}([ATP]) = \alpha_{12} + \beta_{12}[ATP] + \gamma_{12}[ATP]^2 \tag{4b}$$

with the coefficients α_{ir}, β_{ir}, and γ_{ir} chosen so that $\varphi_{11}([ATP])$ and $\varphi_{12}([ATP])$ best satisfy the orthonormal property for a given set of data (25). The first-order component functions themselves were then constructed as weighted sums of the associated basis functions, e.g.,

$$f_1([ATP]) = \lambda_{11}\varphi_{11}([ATP]) + \lambda_{12}\varphi_{12}([ATP]) \tag{5}$$

The second-order component functions were constructed as the weighted sums of products of the associated basis function, e.g.,

$$\begin{aligned} f_{12}([ATP], [CTP]) = {} & \lambda_{11,21}\varphi_{11}([ATP])\varphi_{21}([CTP]) + \\ & \lambda_{11,22}\varphi_{11}([ATP])\varphi_{22}([CTP]) + \\ & \lambda_{12,21}\varphi_{12}([ATP])\varphi_{21}([CTP]) + \lambda_{12,22}\varphi_{12}([ATP])\varphi_{22}([CTP]) \end{aligned} \tag{6}$$

The coefficients λ were determined by least-squares regression.

The component functions were determined sequentially from lower to higher order. The statistical F test was used to identify whether the addition of higher order component functions significantly improved the fit of the HDMR model to the data (i.e., whether the contribution of the component functions was significant). Let $f_A(\boldsymbol{x})$ denote the original RS−HDMR expansion and $f_B(\boldsymbol{x})$ denote a new one obtained by adding an additional component function to $f_A(\boldsymbol{x})$. Define SSE(A) and SSE(B) as the sum of the square error associated with the two approximations

$$SSE(A) = \sum_{j=1}^{300} [f(\boldsymbol{x}_j) - f_A(\boldsymbol{x}_j)]^2 \tag{7}$$

$$SSE(B) = \sum_{j=1}^{300} [f(\boldsymbol{x}_j) - f_B(\boldsymbol{x}_j)]^2 \tag{8}$$

where $\boldsymbol{x}_j$ is the jth NTP concentration combination tested experimentally, $f(\boldsymbol{x}_j)$ is the experimentally observed normalized ATCase activity associated with $\boldsymbol{x}_j$, and the sum is taken over the total number of experimental samples, in this case 300. The ratio

$$F = [(SSE(A) - SSE(B))(300 - p_B)]/[SSE(B)(p_B - p_A)] \tag{9}$$

follows a F distribution with $(p_B - p_A)$ and $(300 - p_B)$ degrees of freedom (df), where p_A and p_B are the total number of parameters for the two approximations. If the observed F given by eq 9 was larger than the tabulated value of the F distribution with $(p_A - p_B)$ and $(300 - p_B)$ df at 99% confidence level, the new component function contained in $f_B(\boldsymbol{x})$ was considered significant, because $f_B(\boldsymbol{x})$ was >99% certain to be a better approximation than $f_A(\boldsymbol{x})$. Otherwise, the new component function was considered insignificant and was not included in the model (32).

The orthogonal property of the HDMR component functions allowed the output variance, σ^2, to be decomposed into its input contributions

$$\begin{aligned} \sigma^2 = {} & \int_{K^4} (f(\boldsymbol{x}) - f_0)^2 d\boldsymbol{x} \approx \int_{K^4} (f_1([ATP] + f_2([CTP]) + \cdots + \\ & f_{12}([ATP], [CTP]) + \cdots)^2 d\boldsymbol{x} = \\ & \int_0^1 (f_1([ATP]))^2 d[ATP] + \int_0^1 (f_2([CTP]))^2 d[CTP] + \cdots + \\ & \int_0^1 \int_0^1 (f_{12}([ATP], [CTP]))^2 d[ATP]d[CTP] + \cdots = \\ & \sigma_1^2 + \sigma_2^2 + \cdots + \sigma_{12}^2 + \cdots \end{aligned} \tag{10}$$

In eq 10, σ_1^2 is the variance explained by the independent effect of $x_1 = [ATP]$, σ_{12}^2 is the variance explained by the pair cooperative action of ATP and CTP, etc. The fraction of the variance explained by the independent effect of ATP is given by σ_1^2/σ^2, by the pair cooperative action of ATP and CTP σ_{12}^2/σ^2, etc.

RESULTS

Initial experiments with single NTPs yielded results consistent with prior literature: ATP enhanced ATCase activity, whereas CTP, UTP, and GTP were all inhibitors. Among the inhibitors, CTP had the largest and most potent effect (○ in Figure 1).

In vivo, the four NTPs are always present in combination with each other. The effects of 300 randomly selected NTP concentration combinations were measured experimentally. The resulting data are provided in Supplementary Table 1 in the Supporting Information. Typical measurement error (as defined by the standard deviation of repeated measurements) was 0.09 normalized activity units (1 normalized activity unit is defined as the activity of ATCase in the absence of any nucleotide).

These data were used to build a RS−HDMR model of ATCase activity (at the fixed tested substrate concentrations) over the four-dimensional NTP input space. ATCase activity was significantly impacted ($p > 0.01$) by six component functions, three of which were first-order (i.e., functions of the concentration of specific NTPs) and three of which were second-order (i.e., functions of the concentrations of two different NTPs). None of the higher order component functions were significant. The complete RS−HDMR model is provided in Table 1. The significant functions were (with the fraction of the variance that they explain given in parentheses): $f_1([ATP])$ (0.40), $f_2([CTP])$ (0.35), $f_3([UTP])$ (0.03), $f_{12}([ATP],[CTP])$ (0.11), $f_{13}([ATP],[UTP])$ (0.008), and $f_{14}([ATP],[GTP])$ (0.004).
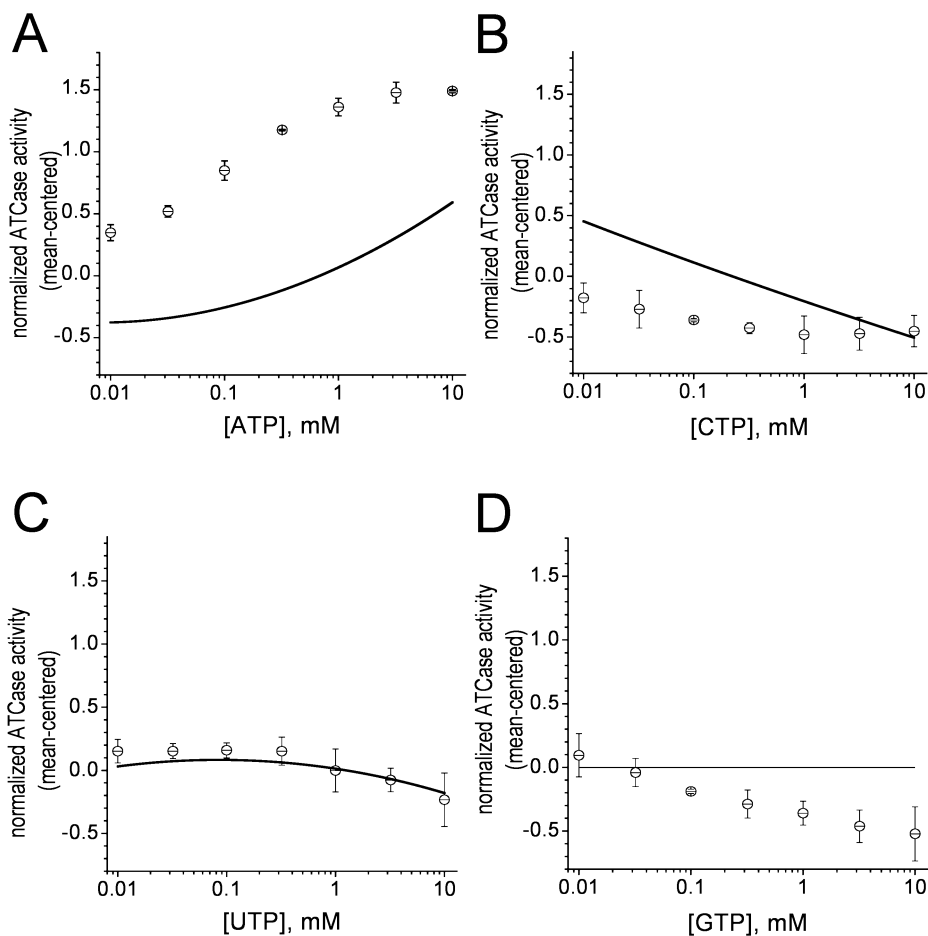
FIGURE 1: Comparison of effects of isolated single NTPs on ATCase activity (○; error bars are ±1 standard deviation of the mean of $N = 2$ measurements) to first-order HDMR functions of the NTPs (—): (A) $f_1([ATP])$, (B) $f_2([CTP])$, (C) $f_3([UTP])$, and (D) $f_4([GTP])$. The y axis shows normalized ATCase activity; one normalized activity unit refers to the activity of ATCase in the absence of any NTP. Consistent with the RS−HDMR framework (in which all component functions are added to the mean measured ATCase activity to obtain the estimated activity), the y axis values are mean-centered: the mean ATCase activity obtained in the experiments involving random concentration combinations of all four nucleotides ($f_0 = 0.78$) has been subtracted from the observed experimental values for the isolated single nucleotides. The use of a thin line to depict $f_4(GTP)$ reflects the lack of a significant first-order effect of GTP.

Table 1: Complete Mathematical Form of the HDMR Model of ATCase Activity

orthonormal basis function	function
$\varphi_{11}([ATP])$	$3.018[ATP] - 1.570$
$\varphi_{12}([ATP])$	$10.257[ATP]^2 - 10.331[ATP] + 1.473$
$\varphi_{21}([CTP])$	$3.090[CTP] - 1.420$
$\varphi_{22}([CTP])$	$10.608[CTP]^2 - 10.515[CTP] + 1.481$
$\varphi_{31}([UTP])$	$2.974[UTP] - 1.496$
$\varphi_{32}([UTP])$	$10.178[UTP]^2 - 10.101[UTP] + 1.356$
$\varphi_{41}([GTP])$	$3.016[GTP] - 1.415$
$\varphi_{42}([GTP])$	$10.345[GTP]^2 - 10.212[GTP] + 1.378$
component function	
f_0	0.775
$f_1([ATP])$	$0.323\varphi_{11}([ATP]) + 0.089\varphi_{12}([ATP])$
$f_2([CTP])$	$-0.310\varphi_{21}([CTP]) + 0.008\varphi_{22}([CTP])$
$f_3([UTP])$	$-0.069\varphi_{31}([UTP]) - 0.054\varphi_{32}([UTP])$
$f_{12}([ATP],[CTP])$	$-0.152\varphi_{11}([ATP])\varphi_{21}([CTP]) + 0.008\varphi_{12}([ATP])\varphi_{21}([CTP]) - 0.041\varphi_{11}([ATP])\varphi_{22}([CTP]) - 0.068\varphi_{12}([ATP])\varphi_{22}([CTP])$
$f_{13}([ATP],[UTP])$	$-0.020\varphi_{11}([ATP])\varphi_{31}([UTP]) + 0.013\varphi_{12}([ATP])\varphi_{31}([UTP]) - 0.032\varphi_{11}([ATP])\varphi_{32}([UTP]) - 0.002\varphi_{12}([ATP])\varphi_{32}([UTP])$
$f_{14}([ATP],[GTP])$	$0.036\varphi_{11}([ATP])\varphi_{41}([GTP]) + 0.017\varphi_{12}([ATP])\varphi_{41}([GTP]) + 0.002\varphi_{11}([ATP])\varphi_{42}([GTP]) - 0.001\varphi_{12}([ATP])\varphi_{42}([GTP])$

The first-order RS−HDMR component functions associated with each NTP are plotted in Figure 1. Except for UTP, these functions differ substantially from the data obtained for the single NTPs in isolation. This implies that the quantitative effects of ATP, CTP, and GTP are strongly modulated by the presence of the three other NTPs. Details of the observed differences and their biological significance are described in the Discussion.

The most significant second-order RS−HDMR component function, corresponding to the ATP × CTP interaction, is plotted in Figure 2A. The function has a complex shape, with the most positive values occurring when ATP is low and CTP is high and the most negative values when ATP and CTP are both high. In interpreting this function, it is important to remember that total ATCase activity (as a function of ATP and CTP) depends upon the sum of the
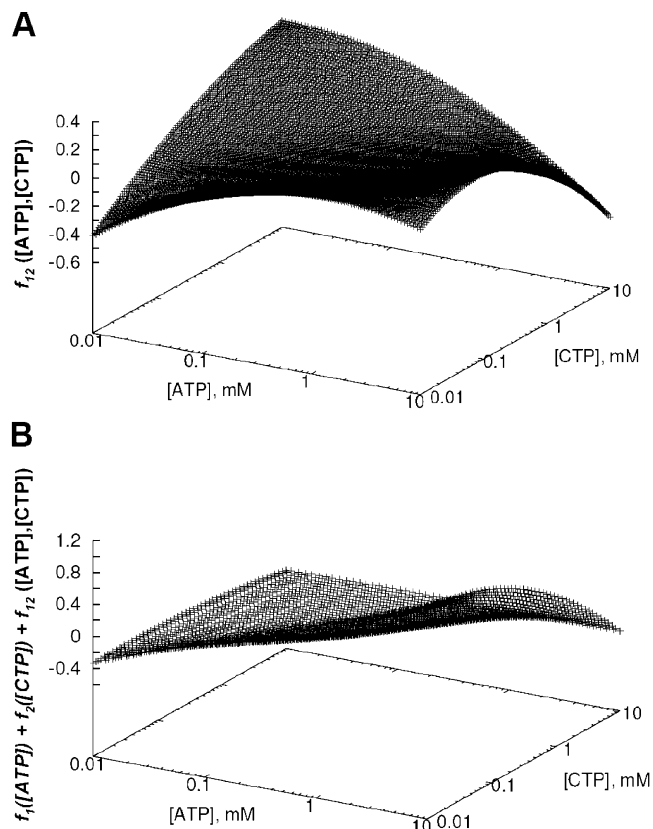
A

B

FIGURE 2: Second-order effect of ATP × CTP. (A) Second-order RS−HDMR component function $f_{12}([ATP],[CTP])$, which reflects the pairwise cooperative effect of the two nucleotides. (B) Best overall estimate of the combined effects of ATP and CTP: $f_1([ATP])$ + $f_2([CTP])$ + $f_{12}([ATP],[CTP])$. z axis units in both panels are normalized ATCase activity (as per the y axis of Figure 1).

A

B

FIGURE 3: Small but statistically significant second-order effects of (A) ATP × UTP: $f_{13}([ATP],[UTP])$ and (B) ATP × GTP: $f_{14}([ATP],[GTP])$. Note that the z axis range is substantially narrower than in Figures 1 and 2, consistent with the minor contribution of the component functions shown here.

first-order effects of ATP and CTP plus this second-order function. Thus, the positive value of the second-order function when ATP is low and CTP is high does not indicate that this ATP × CTP combination maximizes ATCase activity; adding ATP would increase ATCase activity because of the dominant effect of its first-order function (as shown in Figure 2B by a plot of the sum of the first- and second-order functions). The second-order effect is more correctly interpreted as an ability of CTP to overcome ATP: when CTP is high, the ATCase activating effects of increasing levels of ATP are muted. The other second-order functions, while statistically significant, have very small effects. They are shown in Figure 3.

Overall, the RS−HDMR model was successful at describing the data. A truth plot, with predicted ATCase activity on the y axis and measured activity on the x axis, is shown in Figure 4. The model used to generate the truth plot was built using a random set of 200 of the 300 available data points. Most (75%) of the observed data points, including most of those not included in building the model (○) fell within their predicted level ± 2 standard deviations of the experimental measurement error (0.18 normalized activity units; exterior lines). Quantitatively, the high quality of the fit of the model was reflected by the model accounting for 90% of the total variance in the data. The ability of the model to account for 90% of the variance in the data extended also to the 100 data points excluded from model building.
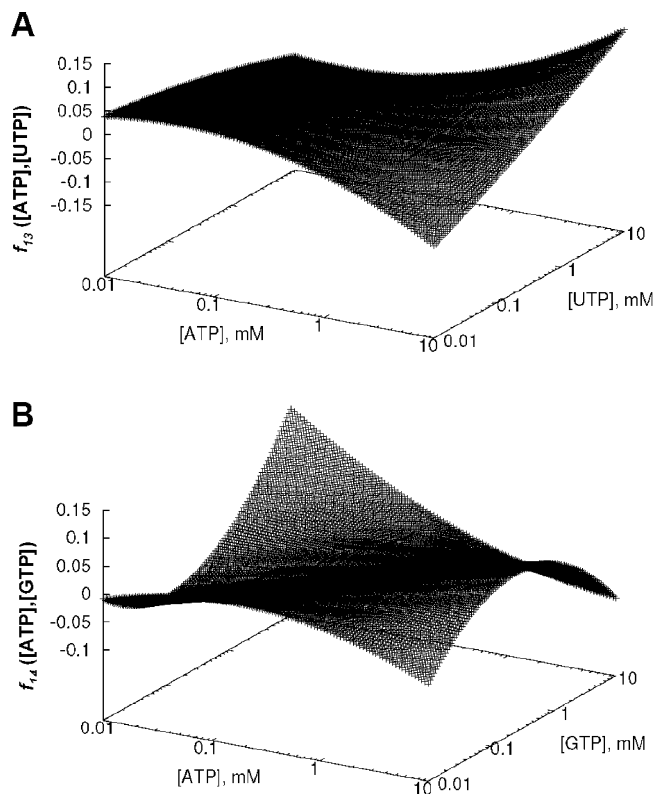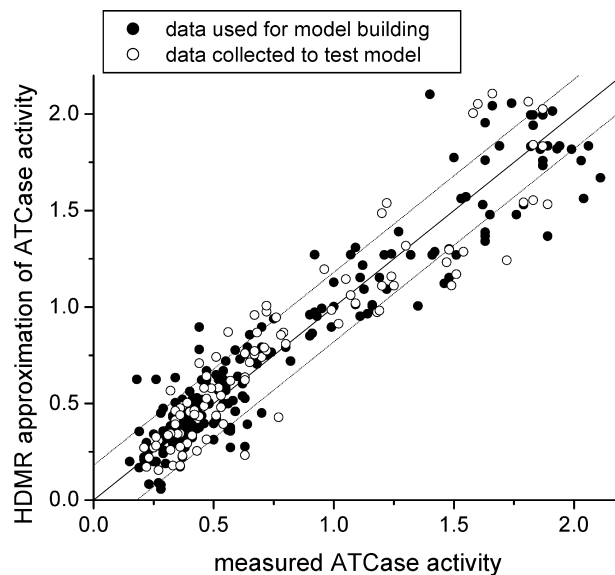

FIGURE 4: Comparison between experimental data and predictions of the RS−HDMR model. The model shown here was built on the basis of data from 200 NTP concentration combinations (●) and tested using the remaining 100 data points (○). The center line is the ideal situation of perfect agreement between model predictions and observed data. The exterior (lighter) lines are approximately 95% confidence limits of the laboratory measurements (±2 standard deviations of a typical measurement).

DISCUSSION

The present paper applies the experimentally driven, statistical modeling approach, RS−HDMR, to investigate

regulation of the well-studied enzyme ATCase in response to varying concentrations of its nucleotide regulators ATP, CTP, GTP, and UTP (at fixed substrate concentrations).

A defining characteristic of RS−HDMR is breaking down a complex function of multiple variables (in this case, ATCase activity as a function of four different NTP regulators) into a sum of generally nonlinear functions of fewer variables. A second-order RS−HDMR model, comprising the sums of functions of single NTPs and pairs of NTPs, described the full four-dimension NTP input space well, as indicated by its capturing of 90% of the variance in the ATCase activity data.

The most significant component functions of the RS−HDMR model reflect the first-order effects of ATP and CTP (parts A and B of Figure 1). Notably, these modeled first-order effects deviate markedly from the effects of ATP and CTP when they are added as single nucleotides in isolation. This reflects the fact that the biochemical effects of ATP and CTP in isolation are quite different from those obtained in the physiological situation of all four nucleotides being present.

Focusing on the circles in Figure 1A, it is evident that addition of ATP alone always results in ATCase activity above the mean activity level found in the presence of all four nucleotides (f_0). In contrast, when other nucleotides are present (−), substantial quantities of ATP are required to reach the mean ATCase activity. This result is consistent with previous literature: ATP activates ATCase, while the other NTPs collectively inhibit it. More interesting is the change in the shape of the ATP response curve in the two cases. When ATP is added in isolation, its effects saturate at ∼1 mM. The typical cellular concentration of ATP is ∼6 mM. Thus, study of ATP in isolation would suggest that ATP is always saturating and, accordingly, not necessarily a physiologically relevant regulator of ATCase. In contrast, the first-order RS−HDMR function of ATP has a different shape, where the effects of ATP are strongest in its physiological range of 1−10 mM (*33, 34*). This difference can be biochemically explained by higher levels of ATP being needed to out-compete the other nucleotides (especially CTP) to drive ATCase into its active R state.

The result with CTP is similar to that with ATP (except with the direction of the effects reversed). Most importantly, whereas the effects of CTP alone nearly saturate at 0.1 mM (well below its reported cellular concentration of 0.5 mM) (*35*), in the presence of the four other nucleotides, there is significant sensitivity to CTP in its physiological range.

For UTP, the single NTP data and the HDMR model closely agree, both showing a weak inhibitory effect, consistent with the presence of a low-affinity UTP-binding site that, when filled, favors the T conformation of the enzyme. For GTP, while the single nucleotide data show an inhibitory effect somewhat stronger than that seen for UTP, the HDMR model shows no effect.

Beyond the first-order component functions of ATP and CTP (f_1 and f_2), the next most significant function was f_{12}([ATP],[CTP]). This indicates the dominant role of ATP and CTP in controlling ATCase activity. While the shape of f_{12} is complex, the most striking trend is for the ATCase-activity-enhancing effects of ATP to be strongest when CTP is low and least when CTP is high (i.e., an ability of CTP to overcome ATP to turn off ATCase). The other significant

second-order effects involved interactions of ATP with UTP and GTP. While weak, the shape of the ATP−UTP interaction is consistent with an ability of ATP to trump UTP to turn on the enzyme. In contrast, the weak ATP−GTP interaction is consistent with an ability of GTP to substitute for ATP to activate the enzyme when ATP is low; when a substantial amount of ATP is present, the effect of GTP is negligible.

Interestingly, the previously reported synergistic interaction of CTP with UTP (*20*) was not found in the present study. This may reflect the current experimental design: some CTP was present in all of the NTP combinations. If only a low concentration of CTP is needed to sensitize ATCase to the inhibitory effects of UTP, then adequate CTP may have been present in all cases, precluding identifying a cooperative effect of the two nucleotides. Whatever the cause of the failure to identify a cooperative effect of UTP and CTP in the present work, the absence of such an effect leads to an important conclusion: such a cooperative interaction, while a characteristic of the interaction of the enzyme with isolated nucleotides, is unlikely to be physiologically significant, because it (unlike the powerful first-order effects of ATP and CTP and negative cooperative effect of ATP × CTP) does not occur at physiologically relevant NTP concentrations.

With respect to such physiological interpretation of the present results, an important limitation of the present work is the use of fixed substrate concentrations. High aspartate levels (>10 mM) can drive ATCase into the R state even in the presence of high CTP and no ATP (*9*). Accordingly, although the tested aspartate concentration was physiological, elevations in intracellular aspartate could presumably override the NTP-mediated regulation studied here.

Typical carbamoyl phosphate levels inside *E. coli* are substantially below the concentration tested here. Despite the relatively low K_m of ATCase for carbamoyl phosphate of ∼200 μM (*36*), they may be subsaturating. Thus, cellular flux through ATCase may be sensitive to the intracellular concentration of carbamoyl phosphate. This concentration reflects not only the activity of carbamoyl phosphate synthetase relative to ATCase but also the rate of consumption of carbamoyl phosphate by the arginine biosynthetic pathway (via ornithine transcarbamoylase). Thus, the present results are inadequate to fully capture physiological regulation of ATCase flux. Nevertheless, partitioning of carbamoyl phosphate consumption between the pyrimidine and arginine pathways will substantially depend upon the rate of the ATCase steps occurring after carbamoyl phosphate binding. Accordingly, the present results regarding regulation of these steps by mixtures of all four NTPs provide a useful addition to studies investigating the effects of single or pairs of NTPs in isolation, as well as to efforts to model the overall activity of the pyrimidine pathway in *E. coli* (*25*).

Beyond providing a more refined understanding of ATCase regulation, the present research also sheds light on the strengths and weaknesses of HDMR as a tool for investigating biochemical systems. A defining attribute of RS−HDMR is its statistical nature: comprehensive estimates of biochemical activity are obtained without regard to the underlying chemical mechanism. RS−HDMR thus provides an unbiased framework for confirming major principles (e.g., the dominant role of ATP and CTP in controlling ATCase activity)

and dissociating them from ancillary observations (e.g., the synergistic effects of CTP and UTP in studies of the two nucleotides in isolation). It also has the potential to lead to unexpected discoveries (e.g., the substantially stronger sensitivity of ATCase activity to physiologically relevant concentrations of ATP and CTP than would have been anticipated from studies of the single nucleotides in isolation). The model-independent nature of RS−HDMR, on the other hand, means that the extracted input−output correlations are not an unambiguous representation of the underlying biophysical mechanism, although the latter can often be deduced by integration of RS−HDMR with biochemical insights and additional targeted experiments.

Accordingly, although no substitute for mechanistic modeling, RS−HDMR has value for studying other enzymes subject to regulation by numerous effectors. In addition, it may prove useful in dissecting other biochemical input−output relationships, both *in vitro* and *in vivo*. Particularly interesting cases involve multiple inputs whose effects are nonlinear and hard to capture via classical mechanistic models. Selected examples include sensitivity of protein folding to different environmental parameters (pH, salt concentration, denaturant concentration, and temperature), cellular transcriptional outputs to combinations of receptor ligands activating different signal transduction cascades, bioreactor yield to feedstock composition, and safety and efficacy of pharmaceutical mixtures to the concentrations of their component-active agents. In certain cases, such as bioreactor yields and pharmaceutical safety and efficacy, the resulting model may be valuable for enabling subsequent optimization of inputs to maximize the desired output.

ACKNOWLEDGMENT

SUPPORTING INFORMATION AVAILABLE

Complete data table in Microsoft Excel format. This material is available free of charge via the Internet at http://pubs.acs.org.

REFERENCES

1. Allewell, N. M. (1989) *Escherichia coli* aspartate transcarbamoylase: Structure, energetics, and catalytic and regulatory mechanisms. *Annu. Rev. Biophys. Biophys. Chem. 18*, 71–92.

2. Gerhart, J. C., and Schachman, H. K. (1965) Distinct subunits for the regulation and catalytic activity of aspartate transcarbamylase. *Biochemistry 4*, 1054–1062.

3. Wiley, D. C., and Lipscomb, W. N. (1968) Crystallographic determination of symmetry of aspartate transcarbamylase. *Nature 218*, 1119–1121.

4. Weber, K. (1968) New structural model of *E. coli* aspartate transcarbamylase and the amino acid sequence of the regulatory polypeptide chain. *Nature 218*, 1116–1119.

5. Porter, R. W., Modebe, M. O., and Stark, G. R. (1969) Aspartate transcarbamylase. Kinetic studies of the catalytic subunit. *J. Biol. Chem. 244*, 1846–1859.

6. Hsuanyu, Y., and Wedler, F. C. (1987) Kinetic mechanism of native *Escherichia coli* aspartate transcarbamylase. *Arch. Biochem. Biophys. 259*, 316–330.

7. Wang, J., Stieglitz, K. A., Cardia, J. P., and Kantrowitz, E. R. (2005) Structural basis for ordered substrate binding and cooperativity in aspartate transcarbamoylase. *Proc. Natl. Acad. Sci. U.S.A. 102*, 8881–8886.

8. Pardee, A. B., and Yates, R. A. (1956) Control of pyrimidine biosynthesis in *Escherichia coli* by a feed-back mechanism. *J. Biol. Chem. 221*, 757–770.

9. Gerhart, J. C., and Pardee, A. B. (1962) The enzymology of control by feedback inhibition. *J. Biol. Chem. 237*, 891–896.

10. Blackburn, M. N., and Schachman, H. K. (1977) Allosteric regulation of aspartate transcarbamoylase. Effect of active site ligands on the reactivity of sulfhydryl groups of the regulatory subunits. *Biochemistry 16*, 5084–5091.

11. Gerhart, J. C., and Schachman, H. K. (1968) Allosteric interactions in aspartate transcarbamylase. II. Evidence for different conformational states of the protein in the presence and absence of specific ligands. *Biochemistry 7*, 538–552.

12. Gibbons, I., Ritchey, J. M., and Schachman, H. K. (1976) Concerted allosteric transition in hybrids of aspartate transcarbamoylase containing different arrangements of active and inactive sites. *Biochemistry 15*, 1324–1330.

13. Johnson, R. S., and Schachman, H. K. (1983) Communication between catalytic and regulatory subunits in Ni(II)- and Co(II)-aspartate transcarbamoylase. Ligand-promoted structural alterations at the intersubunit bonding domains. *J. Biol. Chem. 258*, 3528–3538.

14. Lahue, R. S., and Schachman, H. K. (1986) Communication between polypeptide chains in aspartate transcarbamoylase. Conformational changes at the active sites of unliganded chains resulting from ligand binding to other chains. *J. Biol. Chem. 261*, 3079–3084.

15. Wacks, D. B., and Schachman, H. K. (1985) ^{19}F nuclear magnetic resonance studies of fluorotyrosine-labeled aspartate transcarbamoylase. Properties of the enzyme and its catalytic and regulatory subunits. *J. Biol. Chem. 260*, 11651–11658.

16. Ke, H. M., Lipscomb, W. N., Cho, Y. J., and Honzatko, R. B. (1988) Complex of *N*-phosphonacetyl-L-aspartate with aspartate carbamoyltransferase. X-ray refinement, analysis of conformational changes and catalytic and allosteric mechanisms. *J. Mol. Biol. 204*, 725–747.

17. Kantrowitz, E. R., and Lipscomb, W. N. (1988) *Escherichia coli* aspartate transcarbamylase: The relation between structure and function. *Science 241*, 669–674.

18. Wang, J., Eldo, J., and Kantrowitz, E. R. (2007) Structural model of the R state of *Escherichia coli* aspartate transcarbamoylase with substrates bound. *J. Mol. Biol. 371*, 1261–1273.

19. Monod, J., Wyman, J., and Changeux, J.-P. (1965) On the nature of allosteric transitions: A plausible model. *J. Mol. Biol. 12*, 88–118.

20. Schachman, H. K. (1988) Can a simple model account for the allosteric transition of aspartate transcarbamoylase? *J. Biol. Chem. 263*, 18583–18586.

21. Fetler, L., Kantrowitz, E. R., and Vachette, P. (2007) Direct observation in solution of a preexisting structural equilibrium for a mutant of the allosteric aspartate transcarbamoylase. *Proc. Natl. Acad. Sci. U.S.A. 104*, 495–500.

22. Velyvis, A., Yang, Y. R., Schachman, H. K., and Kay, L. E. (2007) A solution NMR study showing that active site ligands and nucleotides directly perturb the allosteric equilibrium in aspartate transcarbamoylase. *Proc. Natl. Acad. Sci. U.S.A. 104*, 8815–8820.

23. Wild, J. R., Loughrey-Chen, S. J., and Corder, T. S. (1989) In the presence of CTP, UTP becomes an allosteric inhibitor of aspartate transcarbamylase. *Proc. Natl. Acad. Sci. U.S.A. 86*, 46–50.

24. Voet, D., and Voet, J. G. (2004) *Biochemistry*, 3rd ed., John Wiley and Sons, New York.

25. Rodriguez, M., Good, T. A., Wales, M. E., Hua, J. P., and Wild, J. R. (2005) Modeling allosteric regulation of de novo pyrimidine biosynthesis in *Escherichia coli*. *J. Theor. Biol. 234*, 299–310.

26. Rabitz, H., Alis, O. F., Shorter, J., and Shim, K. (1999) Efficient input−output model representations. *Comput. Phys. Commun. 117*, 11–20.

27. Alis, O. F., and Rabitz, H. (2001) Efficient implementation of high dimensional model representations. *J. Math. Chem. 29*, 127–142.

28. Li, G., Hu, J., Wang, S-W., Georgopoulos, P. G., Schoendorf, J., and Rabitz, H. (2006) Random sampling−high dimensional model representation (RS−HDMR) and orthogonality of its different order component functions. *J. Phys. Chem. A 110*, 2474–2485.

29. Yuan, J., Fowler, W. U., Kimball, E., Lu, W., and Rabinowitz, J. D. (2006) Kinetic flux profiling of nitrogen assimilation in *Escherichia coli*. *Nat. Chem. Biol. 2*, 529–530.

30. Nowlan, S. F., and Kantrowitz, E. R. (1985) Superproduction and rapid purification of *Escherichia coli* aspartate transcarbamylase and its catalytic subunit under extreme derepression of the pyrimidine pathway. *J. Biol. Chem. 260*, 14712–14716.

31. Pastra-Landis, S. C., Foote, J., and Kantrowitz, E. R. (1981) An improved colorimetric assay for aspartate and ornithine transcarbamylases. *Anal. Biochem. 118*, 358–363.

32. Chatterjee, S., and Price, B. (1977) *Regression Analysis by Example*, John Wiley and Sons, New York.

33. Buckstein, M. H., He, J., and Rubin, H. (2008) Characterization of nucleotide pools as a function of physiological state in *Escherichia coli. J. Bacteriol. 190*, 718–726.

34. Rabinowitz, J. D., and Kimball, E. (2007) Acidic acetonitrile for cellular metabolome extraction from *Escherichia coli. Anal. Chem. 79*, 6167–6173.

35. Bochner, B. R., and Ames, B. N. (1982) Complete analysis of cellular nucleotides by two-dimensional thin layer chromatography. *J. Biol. Chem. 257*, 9759–9769.

36. Stebbins, J. W., Xu, W., and Kantrowitz, E. R. (1989) Three residues involved in binding and catalysis in the carbamyl phosphate binding site of *Escherichia coli* aspartate transcarbamylase. *Biochemistry 28*, 2592–2600.